A STUDY OF STRAIN EFFECTS IN Ni ALLOYS

Thesis by

Edward Norton Evans

In Partial Fulfillment of the Requirements

For the Engineer's Degree

California Institute of Technology

Pasadena, California

1970

(Submitted September 1, 1970)

Acknowledgements

The author wishes to thank Professors F. B. Humphrey, C. H. Wilts, and T. Vreeland, Jr. for their help. Stimulating discussions with L. W. Brownlow were also appreciated.

Financial support for this work was derived, in part, from the Naval Undersea Research and Development Center and the U. S. Army Research Office.

ABSTRACT

A method for producing uniaxially strained films on an unstrained substrate is described. These films were used to measure the strain sensitivity for γ-phase Ni-Fe and Ni-Co alloys. They were also used to investigate the process of strain relaxation in thin films.

The experimental strain sensitivity was found to be roughly half of the strain sensitivity predicted from bulk material properties for all alloys measured. The strain sensitivity was predicted from bulk magnetoelastic constants by assuming that a film is uniformly strained when its substrate is bent. In the limit of zero thickness, this assumption of a uniform strain is undoubtedly correct. Since no thickness dependence was found for films between 64 and 2800 Å, the uniform strain model should apply to all normal thicknesses. The applied strain sensitivity was found to be independent of strain in agreement with the model of uniform strain. All experimental results are consistent with the assumption that thin film elastic constants are roughly half of bulk elastic constants.

A simple model for uniaxial strain relaxation by volume diffusional creep, roughly predicted the dependence of strain upon annealing time and temperature. A method for determining a single activation energy for the complex process of strain relaxation was found. This activation energy (2.4 ev) is in good agreement with the model used. It was concluded that the dominant mechanism for strain relaxation in thin films is volume diffusional creep.

Table of Contents

Chapter 1

Introduction

1.1 Anisotropy

Magnetic anisotropy in vacuum deposited permalloy thin films was first observed as a preferential alignment of the magnetization along an axis in the plane of the film. Since then, considerable time and effort has been spent attempting to characterize and understand the anisotropy energy in thin ferromagnetic films. The magnitude of the anisotropy energy is mostly dependent upon composition and the substrate temperature at the time of the evaporation. The direction of the easy (preferred) axis can be determined by the application of a magnetic field in the desired direction during evaporation and any subsequent anneal.

Mathematically, anisotropy is most conveniently described by an effective magnetic field. This field can be found by first considering the magnitude of the anisotropy energy given by:

$$E = -K \cos^2 (\theta) \tag{1}$$

where θ is the angle between the magnetization M and the easy axis. Equation 1 can then be used to calculate the position of M at equilibrium in an applied magnetic field. For small values of θ, an effective restoring field H_k, of magnitude 2K/M and parallel to easy axis approximates the equilibrium position of M as obtained from Eq. 1 in the presence of an applied magnetic field. In this paper the angle θ will be defined as the angle between the magnetization and the

direction of the applied magnetic field during evaporation. Thus if the easy axis rotates by 90° from this direction, K in Eq. 1 and consequently H_k will have negative values.

Efforts to understand anisotropy start with known anisotropy producing effects such as preferential crystalline growth, pair ordering, or magnetostriction. Since the crystalline anisotropy is large compared to the anisotropy in a film, it is reasonable that a preferential growth of the crystallites could cause the observed anisotropy in thin films. However, annealing of thin films does not increase the observed anisotropy but does increase the crystallite size[1], thus making it unlikely that preferential growth is a cause of anisotropy. Pair ordering, the preferential alignment of AB pairs of atoms in an AB alloy, has been shown to cause anisotropy in bulk materials. This could explain part of the anisotropy in all alloys but not in pure metals, where the anisotropy can be large. Here and at magnetostrictive alloys, the anisotropy could be caused by magnetostriction. A uniaxial strain in a magnetostrictive film is known to induce an anisotropy.[2] Thus in magnetostrictive films constrained by their substrates, it is reasonable to assume that the substrate constraint will produce a magnetostrictive anisotropy.

The total anisotropy in thin films was assumed by Robinson[3] to be the sum of the magnetostrictive anisotropy and pair ordering anisotropy. He then calculated the magnetostrictive component of the total anisotropy by assuming that the substrate constraint imposes a stress $\lambda' E$, where E is Young's modulus and λ' is the average saturation magnetostriction constant at a temperature T'. The temperature T' is

the temperature at which the film becomes constrained by the substrate as it cools. The anisotropy resulting from a uniform stress $\lambda'E$ is given by:

$$K_s = -\frac{3}{2}\lambda\lambda'E. \qquad (2)$$

where K_s is the anisotropy constant in Eq. 1 due to magnetostriction. Using Eq. 2, Robinson attempted to show that the magnetostrictive anisotropy component is small in the composition range 40%-100% Ni-Fe, except near 50% and 100% Ni.

A more detailed model for the magnetostrictive anisotropy was calculated by West[4], who argued that Robinson's calculation was incorrect in principle and that its prediction for pure Fe (where no pair ordering exists) was in severe disagreement with experiment. West assumed that each individual crystallite was deposited in equilibrium. The magnetoelastic elongation in the direction of the initial magnetization was calculated from the magnetoelastic energy expression given by Kittel.[5] Each crystallite was assumed to be constrained by the substrate in this equilibrium position. The magnetostrictive anisotropy energy for a single crystallite was then calculated from its equilibrium elongation. By averaging this anisotropy energy over all orientations of crystallites with respect to the initial magnetization, the magnetostrictive anisotropy energy for a polycrystalline film was obtained. Unfortunately, when West used his result to predict the magnetostrictive anisotropy at pure Co, he predicted nearly twice the measured anisotropy.

1.2 Magnetostriction

Uniaxially strained films can be obtained by bending the substrate over two knife edges. The strain induced between the knife edges can then be calculated by assuming that the substrate bends like a homogeneous beam with its ends on free supports and the center plane remaining unstrained. The deflection of such a beam with a force F applied at a distance a from each end can be found by the superposition of the results for each force alone. The deflection due to a single force is given by:

$$y(x) = Fbx\ [2L(L-x)-b^2-(L-x)^2]\ /\ 6EIL \qquad (3)$$

where E is Young's modulus, I is the moment of inertia of the cross sectional area of the substrate with respect to the neutral axis, L is the length of the beam, a + b = L, and x is measured from the ends to the point where the force is applied. The force is unknown experimentally and is proportional to the strain between the knife edges which is given by:

$$e = FaT/2EI \qquad (4)$$

where T is the thickness of the substrate. The experimentally controlled parameter is the deflection of the knife edges, which is:

$$y(a) = Fa(2Lb^2-b^3+2Lab-a^3-ab^2)\ /\ 6EIL \qquad (5)$$

from Eq. 3. This can be used to eliminate F/EI from Eq. 4 and give the strain between the knife edges in terms of the deflection at the knife

edges as:

$$e = 3Ly(a)T/(3ab^2+2ba^2+a^3). \tag{6}$$

Outside the knife edges the strain drops linearly to zero with the distance to the end of the substrate.

The average strain must be calculated when the film extends beyond the bending knife edges where the strain is not uniform. For a circular film of radius r and angle i between a line through the center of the film perpendicular to the bending knife edges and a line through the center of the film intersecting the film's perimeter at one of the bending knife edges, the average strain is given by:

$$\bar{e} = e\left[(2i-\sin^2 i)\left(\frac{L}{2a}-1\right)/\pi + 1 - \frac{4r\sin^3 i}{3\pi a}\right] \text{ where}$$

$$i = \cos^{-1}\{L/(2r)-a/r\} \tag{7}$$

where e is the strain in the center region given by Eq. 6. For the geometry used in this experiment, Eq. 7 gives $\bar{e}$ = .935 e for two knife edge bending and $\bar{e}$ = .66 e for one knife edge bending by letting i go to $\pi/2$.

The anisotropy induced by the average strain is reasonably approximated as that produced by a uniform strain of equal magnitude and can be calculated from the magnetoelastic equation given by Kittel[5]. Let a_i be the direction cosine of the magnetization in the i direction and e_{ij} be the elements of the strain tensor with respect to the cubic crystal axes, then the magnetoelastic energy is given by:

$$E = B_1 [e_{xx}(a_1^2-1/3)+e_{yy}(a_2^2-1/3)+e_{zz}(a_3^2-1/3)] \quad (8)$$

$$+ B_2 (e_{xy}a_1a_2+e_{yz}a_2a_3+e_{zx}a_3a_1) \quad \text{where}$$

$$B_1 = 3/2 (c_{11}-c_{12})\lambda_{100}$$

$$B_2 = 3c_{44}\lambda_{111}.$$

Since deformations perpendicular to the plane of the film do not contribute to the anisotropy in the plane of the film, no Poisson contraction will be allowed perpendicular to the plane of the film. Thus the strain tensor for a uniform strain e can be written for all i and j as:

$$e_{ij} = eg_ig_j (2-\delta_{ij}) \quad (9)$$

where the g_i's are the direction cosines of the strain relative to the crystal axes. Substituting Eq. 9 into Eq. 8 and averaging over all angles holding the angle m between the magnetization and the strain constant, the magnetoelastic energy becomes:

$$E = \frac{e}{5} [2B_1\cos^2(m) + 3B_2\cos^2(m) + \text{const.}]. \quad (10)$$

For the magnetization in equilibrium with this strain anisotropy energy, an effective strain anisotropy field can be calculated using the techniques previously used with the phenomenological anisotropy (Eq. 1) to be:

$$H_{ks} = \frac{3e}{5M} [2 (c_{11}-c_{12})\lambda_{100}+6c_{44}\lambda_{111}]. \quad (11)$$

The strain anisotropy field, H_{ks}, is directly proportional to the strain

which leads to the definition of the strain sensitivity, s, as H_{ks}/e.

A model assuming a uniform stress has been used by several investigators[2,6]. This model yields the result:

$$H_{ks} = 3\lambda S/M \tag{12}$$

where λ is the average magnetostriction, M the saturation magnetization, and S the applied stress. Assuming that $S = E\bar{e}$ and expressing λ in terms of λ_{100} and λ_{111}, this expression can be written as:

$$H_{ks} = \frac{3\bar{e}E}{5M} (2\lambda_{100} + 3\lambda_{111}) \tag{13}$$

where $\bar{e}$ is the average strain and E is Young's modulus. By experimentally interpreting $\bar{e}$ as the strain induced by the bending of the substrate, Eq. 13 can be used to calculate the strain sensitivity from known bulk constants.

Experimentally, the strain sensitivity is the only measurable parameter for thin magnetic films which can be easily interpreted in terms of the magnetostriction constants. Thus unless single crystal samples are used, only a sum of λ_{111} and λ_{100} can be calculated from s by either Eq. 11 or 13, knowing the elastic constants and M. The strain sensitivity can be measured by applying a uniaxial strain either parallel or perpendicular to the easy axis and measuring the change in H_k which results. Since the resulting change in H_k is equal to the strain induced anisotropy field, then $s = \pm \Delta H_k/e$ where the plus sign is for a strain along the easy axis and the minus sign is for a strain along the hard axis.

1.3 Annealing

Mechanisms of strain relaxation in polycrystalline thin films were discussed from a theoretical point of view by Chaudhari[7]. Considering thin films under uniaxial stress, Chaudhari concluded that mechanisms involving dislocation motion and grain boundary sliding were not the dominate mechanisms for strain relaxation in films of thicknesses comparable to the grain diameter. Diffusional or Nabarro-Herring[8] creep was concluded to be the most probable mechanism for strain relaxation by annealing. Diffusional creep occurs by the motion of vacancies under a concentration gradient generated by the applied stress. This concentration gradient is generated by changes in the activation energy for formation and annihilation of vacancies with applied stress. Thus the probability of finding a vacancy at a given site under a stress S is assumed to be:

$$P = e^{-E_f/kT}\, e^{SV/kT} \tag{14}$$

where E_f is the free energy of formation of a vacancy and V is the volume of a vacancy. By assuming that grain boundaries are sources and sinks of vacancies, the plastic strain rate is given by:

$$de/dt = He^{-E_s/kT}(e^{SV/kT}-1) \tag{15}$$

where $H = B/dh$ if volume diffusion is dominant and $H = B'/dh^2$ if grain boundary diffusion is dominant. Here B and B' are constants which can be determined[9], h is the height of the grain, d is the diameter of the grain, and E_s is the self-diffusion activation energy for either grain boundary (2 ev) or volume (3 ev) diffusion.

Stress relaxation experiments done on thin iron films by Finegan and Hoffman[10] were not interpreted in terms of the mechanisms discussed by Chaudhari. A large isotropic stress was found to exist in thin evaporated films, for which the magnitude was calculated from the deflection of the substrate due to the stress in the film. By consecutive fifteen minute anneals at 25°C increments, the annealing temperature dependence of this isotropic stress was measured (at room temperature). Experimentally, it was found that the isotropic stress decreased with increasing annealing temperature to a minimum value near 425°C and then began increasing. This anomalous behavior could not be explained by the authors.

Chapter 2

Experimental

2.1 Film Preparation

All films were made by vacuum evaporation of Ni alloys onto cleaned glass substrates of known temperature. The glass substrates were cleaned with chromic acid cleaning solution, acetone, distilled water, and methyl alcohol in an ultrasonic cleaner, then baked in the vacuum ($<10^{-6}$ Torr) for at least one hour at or above the evaporation temperature before evaporation. The temperature of the substrate was controlled by maintaining the temperature of the mask which holds the substrates within $\pm$ 5°C and the shutter underneath the substrates within $\pm$ 10°C of the desired temperature.

The thickness of the films was controlled by the shutter assembly while the evaporation rate was held constant at 10 Å per second. The shutter was designed with a slot wide enough to allow each of three rows of four films to be made independent of others or to expose all twelve films at the same time. A quartz crystal thickness gauge was used to monitor the thickness.

The magnetic character of the resultant film is strongly dependent upon the temperature of the substrate during evaporation. When the shutter is opened the substrate changes temperature by radiation. This change continues throughout the evaporation. It can be estimated by taking the solid angle divided by 4π which is subtended by the melt b, by the room a, and by the substrate holder (1-a-b) and calculating the

net radiated power incident on the substrate. This is given by:

$$P = k((1-a-b)T_e^4 + aT_r^4 + bT_m^4 - T_s^4) \qquad (16)$$

where k is related to the Stefan-Boltzman constant, T_r is room temperature, T_e is the temperature of the substrate holder, T_s is the temperature of the substrate, and T_m is the temperature of the melt. Here it is assumed that the substrate is a black body and that no heat is conducted through the metal-glass interfaces supporting the substrate which have very low conductivity. The temperature differential from one side of the substrate to the other is also neglected since if the total power incident on one surface were conducted through the substrate, it would be less than 6°C for glass of conductivity 10^{-3}cal/cm/sec/°C (a low value for glass) and create an error of less than 3°C. The solution of Eq. 16 for P = 0 gives the equilibrium temperature of the substrate as a function of the temperature of the film holder. This result is plotted in Fig. 1 as a solid curve for T_m = 1350°C. A dashed curve was drawn to represent the temperature of the substrate before the shutter is opened. The actual temperature of the substrate will always be between the two curves. Thus when data are presented in Fig. 9, the evaporation temperature will be given as the temperature of the substrate holder and the error bar will be the deviation of this temperature from the equilibrium temperature plus the 5°C error due to the temperature controller.

2.2 Substrate Holder

Films were strained by bending the substrate over tungsten wires before the evaporation of the film and then releasing the substrate

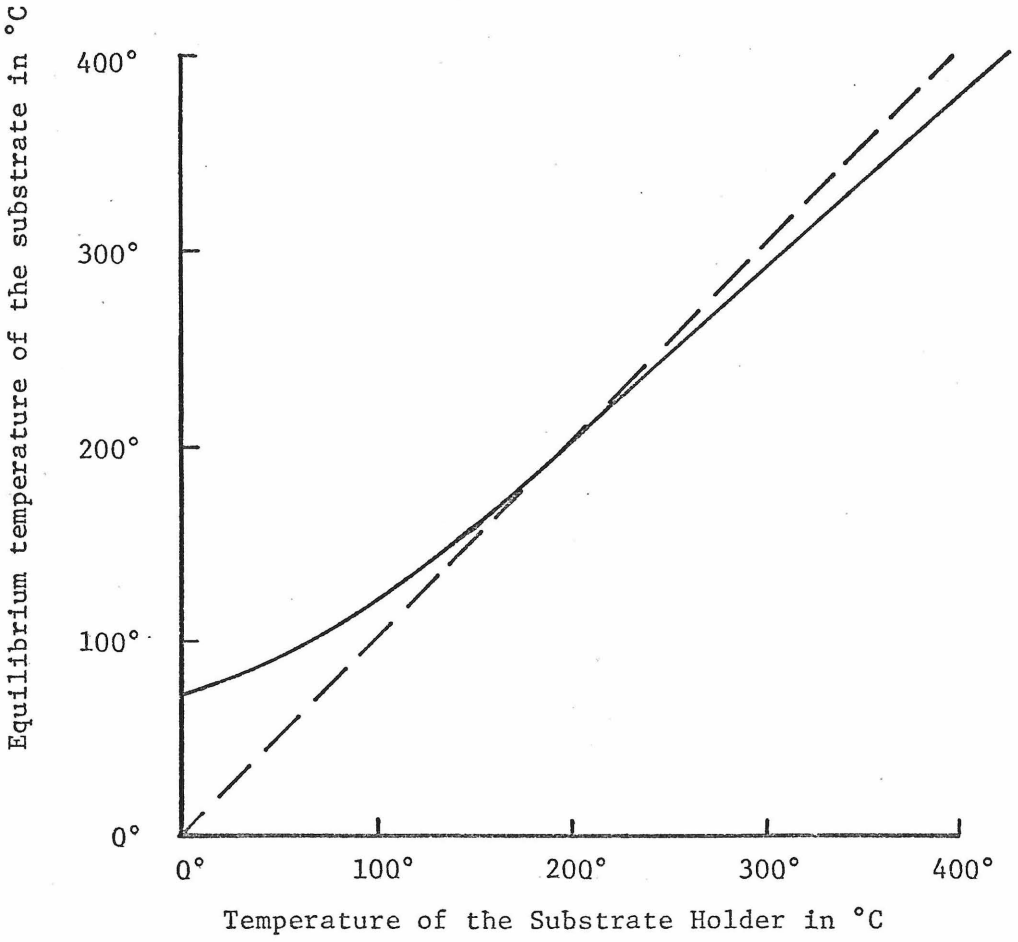

Fig. 1. The equilibrium temperature of the substrate with the shutter open (solid curve) and with the shutter closed (dashed curve).

after evaporation. Two 18 mil tungsten wires were placed in slots marked A in Fig. 2 to support the outside edges of the substrate. The substrate was then put in place and either one or two smaller wires, between 1 and 8.1 mil, were then placed in slots marked B or C respectively. A copper block was then placed on top of the small wires and forced downward by a screw mechanism until the edges of the substrate were pinned between the 18 mil wires in slots A and the copper block. The deflection at slots B or C was then known to be the diameter of the smaller wires and was used with Eqs. 6 and 7 to predict the strain in the film after the substrate was released, the film being deposited in an unstrained condition on the strained substrate.

All strained films were made with two 3-mil wires (which gives the maximum obtainable strain, 5.1×10^{-4}), without breaking any substrates, except for specific experiments where different strains were required. When different strains were required in a single evaporation, three films were made at each of three different strains with three films remaining unstrained to serve as controls. A single wire was sometimes used, which allowed a greater variety of strains (1.3×10^{-4} to 1.04×10^{-3}), to be produced from commercially available wire sizes.

Experimentally, the radius of curvature between the bending wires was checked on three films. The bent glass substrates were used as mirrors. A distant object of width w was made to appear the exact size of the separation between the bending wires s by adjusting the distance between the object and the substrate d. The object was nearly perpendicular to the substrate and was viewed from a measured distance L, also

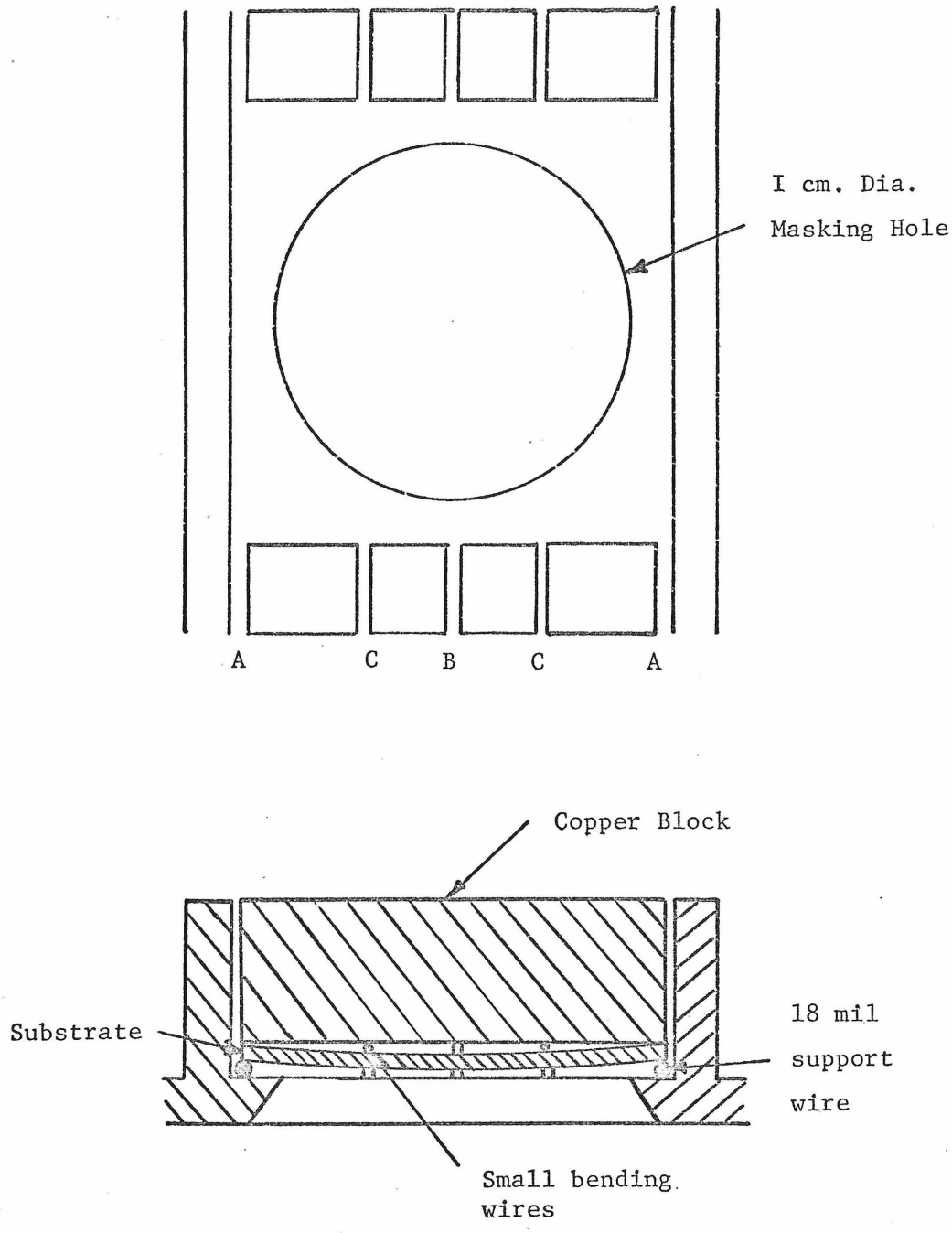

Fig. 2. The substrate holder which was used to bend the substrate.

nearly perpendicular to the substrate. Assuming that both the object and the viewer were perpendicular to the substrate, the radius of curvature is given by:

$$R = 2sLd \; / \; [Lw-(L+d)s] \tag{17}$$

where small angle approximations are used. The average experimental result was R = 7.1 inches. This is within 2% of the result calculated (7.2 in.) by using Eq. 6 and the fact that R = T/2e where e is the strain and T is the thickness of the substrate. Thus the strain calculations are experimentally verified.

2.3 Annealing

Vacuum anneals were made at pressures less than 7×10^{-7} Torr in a copper cavity. The temperature stability of the cavity was $\pm$ 5°C and heating and cooling rates of 30°C/min. were obtained. During each anneal, the temperature was held constant for 3 hours. Each set of sixteen films was annealed at consecutively higher temperatures, normally 25°C intervals.

Silicone oil anneals were also done. Here a circulating temperature controlled bath was used to keep the temperature constant within 1°C, using time as the variable. The films were immersed in the hot oil for the desired length of time and then quickly removed and immersed in a room temperature bath of oil. The error in time was not greater than one second. All anneals were done in a magnetic field parallel to the direction of the field during deposition.

2.4 Measurements

The film composition was obtained from the melt composition by use

of a calibration curve determined by x-ray fluorescence. Due to fractionation, the film composition varies as much as 15% from the melt composition for Ni-Fe alloys and less than 1% for Ni-Co alloys. Thus no correction was used for Ni-Co alloys giving an error less than 1%. However, for Ni-Fe alloys where the calibration curve was used, the uncertainty was a maximum near 50% Ni of 2% and decreased to zero at pure Ni.

The film thickness was determined from the height of the hysteresis loop. The amplitude of the hysteresis loop was also calibrated by optical thickness measurement on a number of films. The uncertainty of the measurements in thickness were less than 5%.

All values of H_k were determined on a hysteresis loop tracer by use of Kobelev's method[11]. A consistency better than 3% was obtainable with an accuracy better than 10%. All measurements were made at room temperature.

Chapter 3

Magnetostriction Measurements

3.1 Introduction

The magnetostrictive anisotropy in thin films has been predicted by West and by Robinson. The total anisotropy was assumed by Robinson to be the sum of the magnetostrictive anisotropy and the anisotropy due to pair ordering. West argued that the magnetostrictive anisotropy component predicted by Robinson is not correct in principle and then calculated a more accurate magnetostrictive anisotropy by averaging the single crystal magnetoelastic energy over a polycrystalline aggregate. West then predicted the magnetostrictive anisotropy for Ni, Fe, and Co where no pair ordering anisotropy exists. His prediction for the magnetostrictive anisotropy component was a clear improvement over Robinson's prediction for Fe. However, for Ni and Co, both models predicted significantly larger anisotropies than are found experimentally. In an attempt to measure the magnetostrictive anisotropy directly, Brownlow and Wilts[12] measured the change in anisotropy upon removal of a film from its substrate. To the extent that crystallites in a free film are not interacting, this change in anisotropy is the same as the magnetostrictive anisotropy component discussed by West and Robinson. They then concluded from their data for Ni-Co and Ni-Fe alloys that neither West nor Robinson correctly predict the anisotropy component which was measured.

Both West's and Robinson's models rely on bulk magnetoelastic constants which do not necessarily apply to thin films. Thin films

contain high vacancy concentrations and large isotropic stresses which could significantly change the magnetoelastic constants. Thus the predicted magnetostrictive anisotropy may be significantly different when thin film magnetoelastic constants are used. These constants can be estimated from measurements of the strain sensitivity. By evaporating films on bent substrates and releasing the substrates after the evaporation, Ni-Fe and Ni-Co films can be uniaxially strained by an amount which can be calculated from the deflection of the substrate previous to evaporation. From measurements of the strain induced anisotropy, the experimental strain sensitivity can be determined and then the magnetoelastic constants estimated by the use of Eq. 11.

3.2 Strain Dependence of s

The anisotropy of thin films of various compositions was measured for various strains. Figure 3 shows typical results for H_k as a function of both positive and negative strains in 85% Ni-Fe films. Positive values of strain were achieved by compressing the film perpendicular to the applied magnetic field during evaporation. For both positive and negative strains each data point represents the average of three films. The line which best fits the data has a slope equal to the average strain sensitivity of all forty-five films measured. The observed linear dependence of H_k on strain implies that the strain sensitivity is constant. The strain sensitivity was also found to be independent of strain at five other compositions between 76% Ni-Fe and 50% Ni-Fe.

No data were taken in the region near $H_k = 0$ where an anomaly was

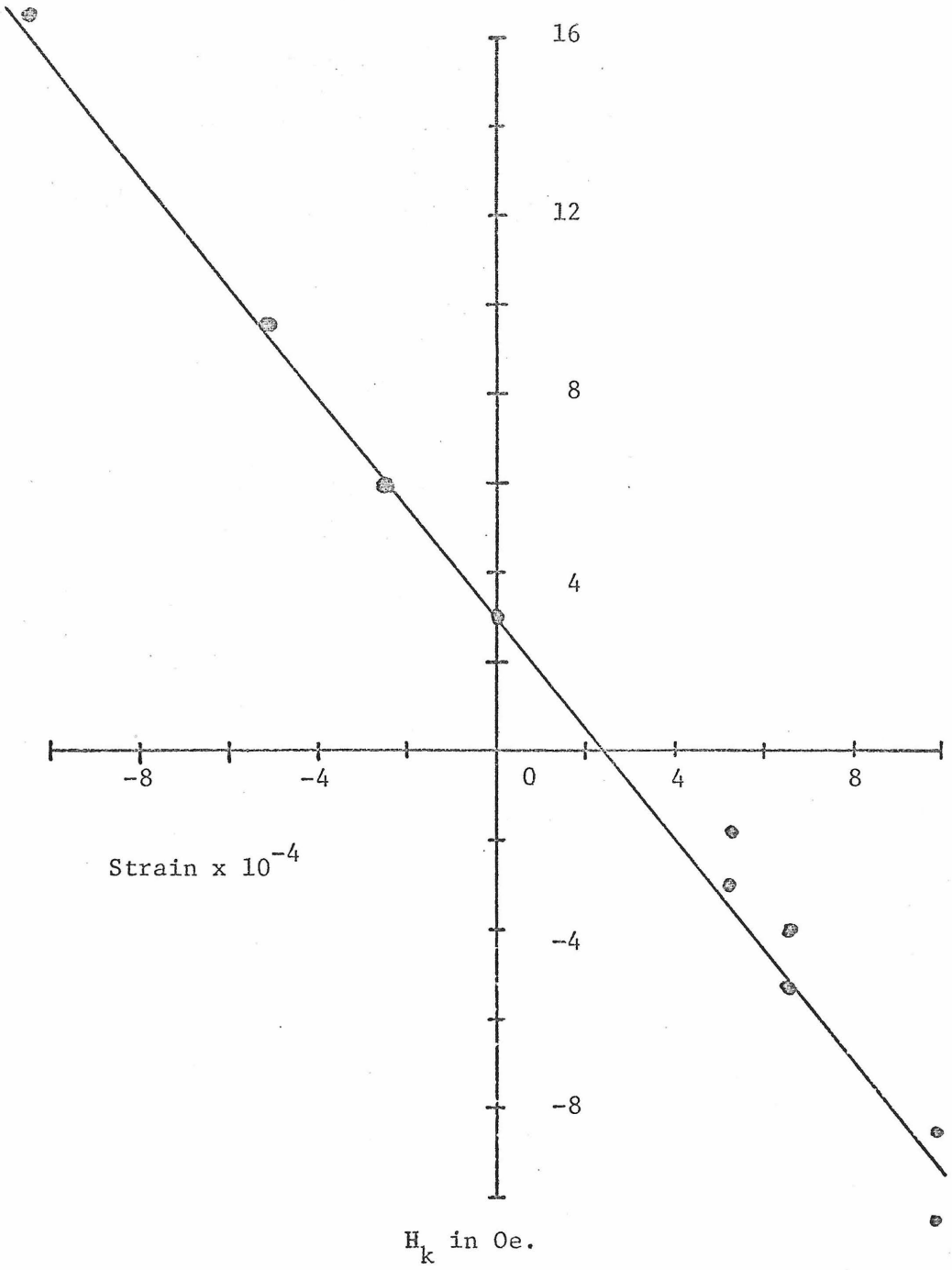

Fig. 3. H_k as a function of Strain for 85-15% Ni-Fe films with 3 films per data point.

discovered. The anisotropy field magnitude never actually goes to zero. It reaches a minimum value between .2 and 2 oe and then the easy axis rotates by 90° at this roughly constant magnitude of anisotropy. Thus measurements of the magnitude of H_k in this region are not consistent with the interpretation of the other data and were excluded from Fig. 3.

3.3 Compositional Dependence of s

The compositional dependence of the strain sensitivity can be predicted from bulk magnetoelastic constants by the use of either Eq. 11 or Eq. 13. Equation 11 predicts the anisotropy induced by a uniform strain and Eq. 13 predicts the anisotropy induced by a uniform stress. If a homogeneous material like glass is used as a substrate, then the top surface will be uniformly strained when the substrate is bent. Thus in the limit of zero thickness, a film which is rigidly bonded to the substrate will be uniformly strained by bending the substrate. For very thin films then, the strain sensitivity should be correctly predicted by Eq. 11. Moreover, experimentally no thickness dependence of s was found for films from 64 to 2800 Å. Thus the assumption of a uniform strain and the use of Eq. 11 to predict the strain sensitivity should be used for all films in the thickness range normally considered.

Thin films with γ-phase crystallites will be used when comparing experimental and predicted values of s, since available bulk magnetoelastic constants[13,14,15,16] are for γ-phase single crystals. Gamma-phase crystallites exist in Ni-Fe alloys between 40% Ni-Fe and 100% Ni for an evaporation temperature between 25°C and 300°C[17]. For Ni-Co alloys evaporated between 25°C and 300°C, the γ-phase region increases in width with increasing evaporation temperature. Thin films

evaporated at 25°C have γ-phase crystallites between 60% Ni-Co and 100% Ni, while films evaporated at 300°C have γ-phase crystallites between 30% Ni-Co and 100% Ni. Outside these regions mixed crystal phases exist. Experimentally, 300°C was the highest evaporation temperature at which strained films could be reliably made. Thus 300°C evaporation temperature is used for Ni-Co alloys.

The experimental strain sensitivity is plotted as a function of composition for Ni-Co alloys in Fig. 4. A solid curve was drawn to best fit the experimental data, where each data point (X) represents the nine strained films from a single 300°C evaporation. The strain sensitivity predicted from bulk data by use of Eq. 11 is represented by a dashed curve. For reference, the data taken for 25°C evaporation temperature are presented(the dots), where each dot represents the nine strained films of a single evaporation. The 25°C data are opposite in sign from the 300°C data at 20% Ni-Co as might be expected from the differences in crystal structure. Both evaporation temperatures have γ-phase crystallites at 70% and 80% Ni-Co. Here the differences in s between the two evaporation temperatures is slightly more than can be attributed to experimental scatter.

For Ni-Fe alloys no dependence of s upon evaporation temperature was found within the limits of the 20% experimental scatter. Therefore all evaporation temperatures for the γ-phase Ni-Fe alloys were compiled to plot s as a function of composition in Fig. 5. Most of the data was taken at either 25°C or 200°C evaporation temperature. The nine strained films from a single evaporation are represented by each data point. A

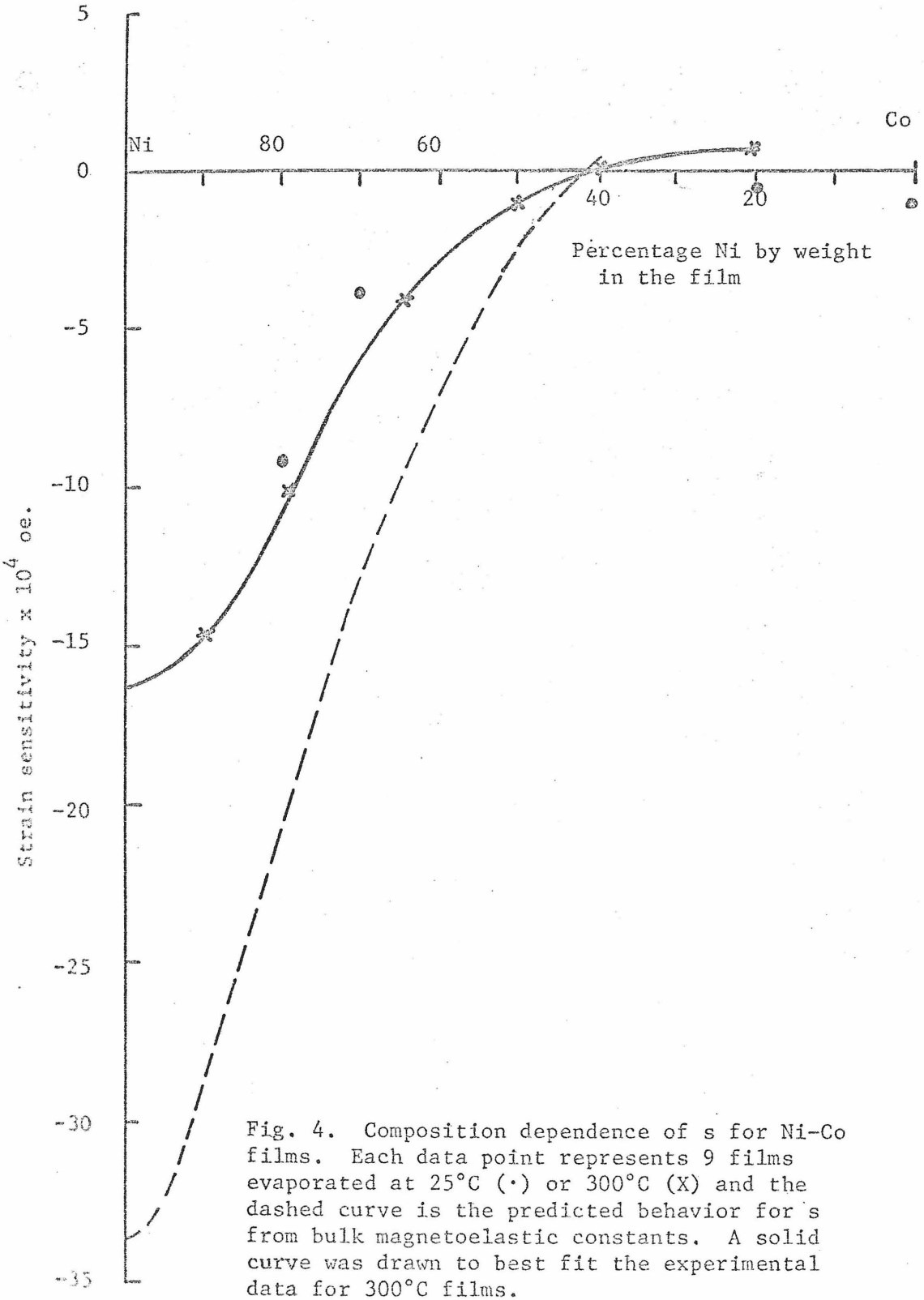

Fig. 4. Composition dependence of s for Ni-Co films. Each data point represents 9 films evaporated at 25°C (·) or 300°C (X) and the dashed curve is the predicted behavior for s from bulk magnetoelastic constants. A solid curve was drawn to best fit the experimental data for 300°C films.

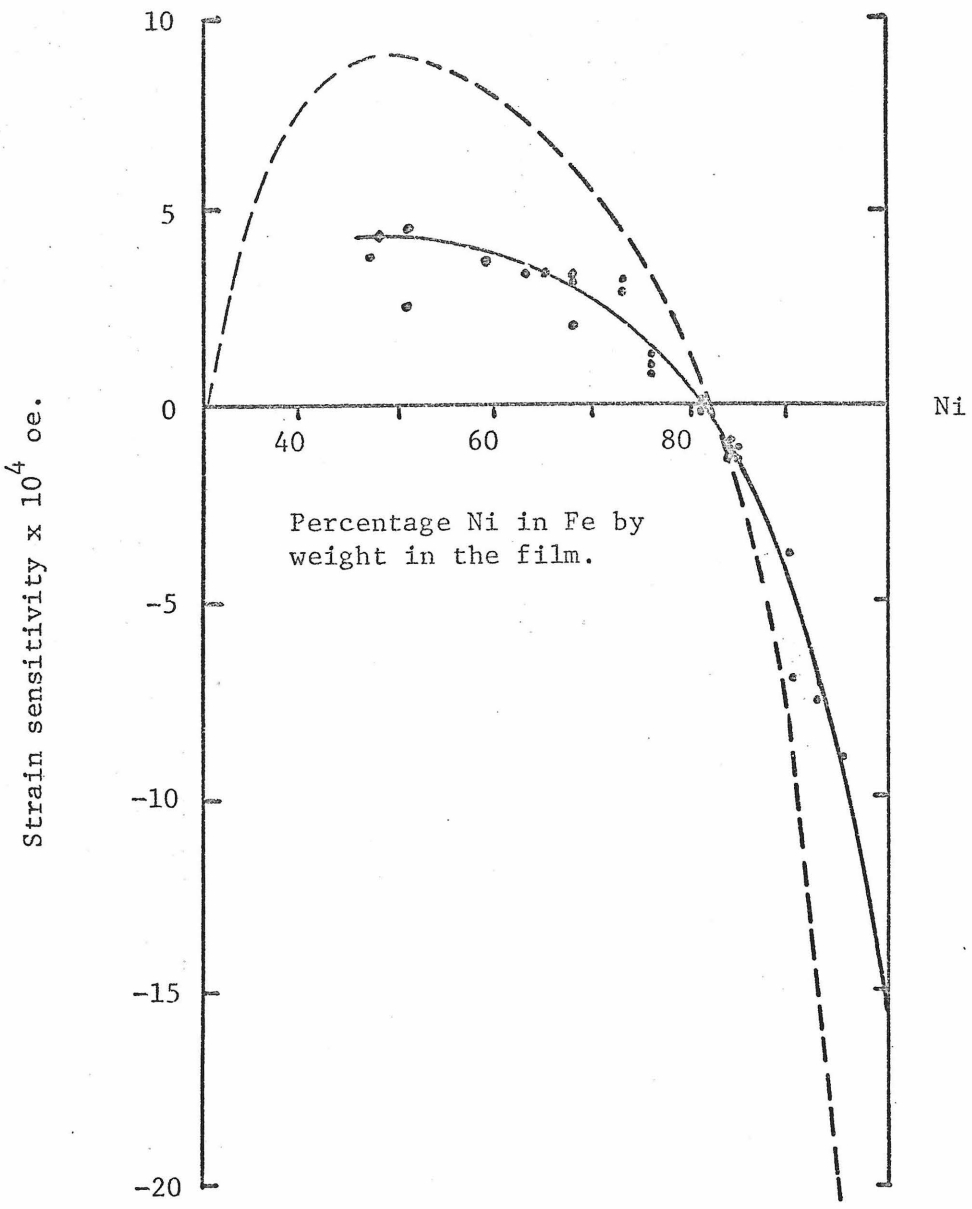

Fig. 5. Composition dependence of s for Ni-Fe γ-phase films. Each data point represents 9 films and the dashed curve is the predicted behavior for s from bulk magnetoelastic constants. A solid curve was drawn to best fit the experimental data.

solid curve was drawn to best fit the experimental data and was extrapolated to pure Ni to best match an extrapolation of the Ni, Co data in Fig. 4. The predicted strain sensitivity using bulk data and Eq. 11 is represented by a dashed curve.

The experimental strain sensitivity from Figs. 4 and 5 is easily seen to be roughly 50% of that predicted for all compositions measured. This is more clearly seen in Fig. 6, where the predicted strain sensitivity is plotted to half scale. Here the solid curves are the solid curves drawn through the experimental data in Figs. 4 and 5 and the dashed curve is the predicted strain sensitivity plotted to half scale. Since the predicted strain sensitivity from Eq. 11 involves the products of the magnetostriction constants and the elastic constants for single crystals, by reducing either the magnetostriction or the elastic constants for bulk material by a factor or two for all compositions, thin film magnetoelastic constants can be derived which accurately predicted the experimental strain sensitivity. The elastic constants are relatively independent of composition while the magnetostriction constants change rapidly with compositional changes. The elastic constants are known to change when imperfections are annealed in bulk material. The high concentration of vacancies in thin films could produce such effects. Thin films also contain isotropic stresses[10] near the elastic limit of bulk material. Such stresses in bulk material would change the elastic constants. It is thus reasonable to conclude that bulk elastic constants are roughly twice the magnitude of thin film elastic constants.

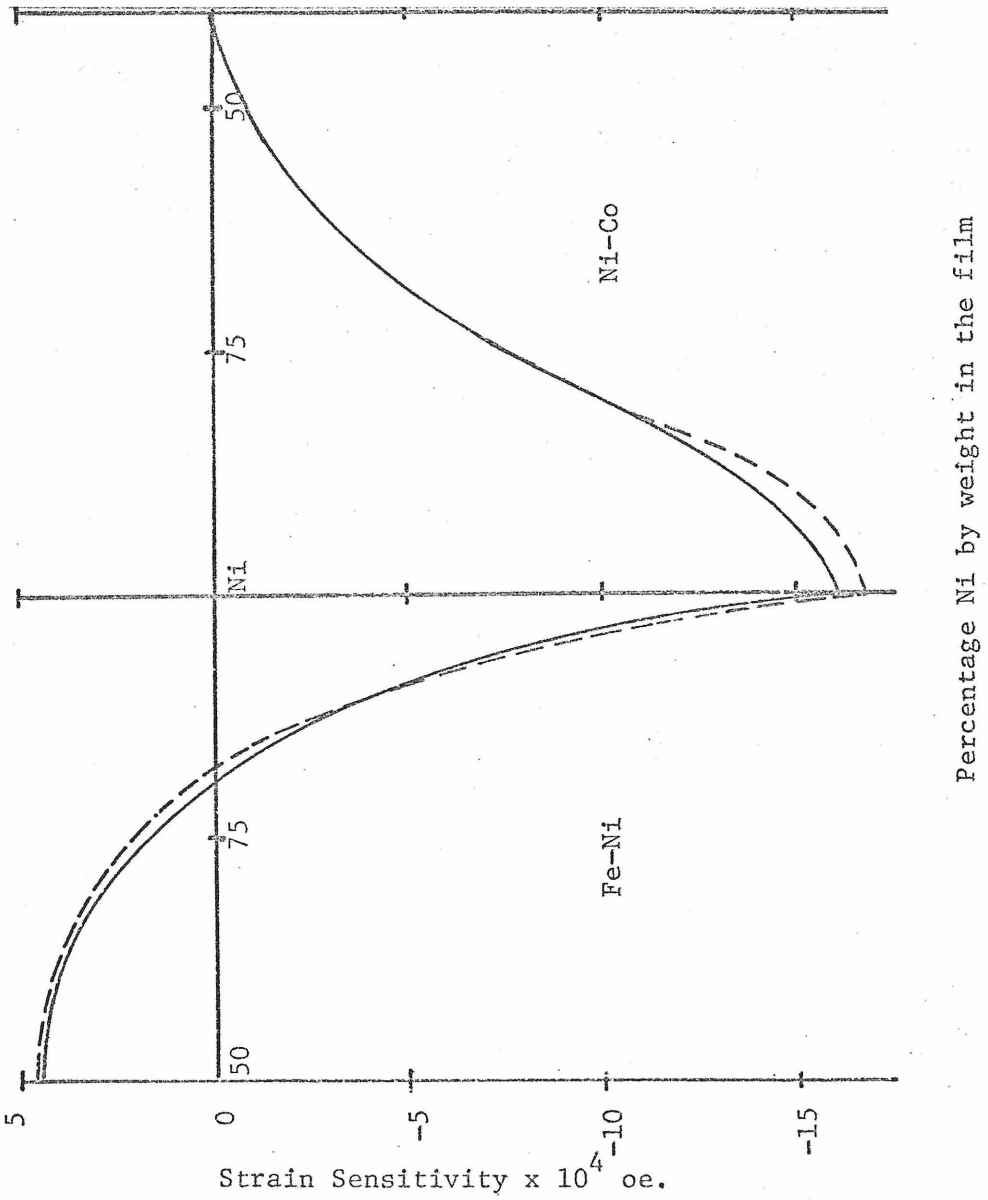

Fig. 6. Strain sensitivity for γ-phase Ni alloys. The solid curve is the best fit to the experimental data from Figs. 4 and 5 and the dashed curve is half the strain sensitivity predicted from bulk magnetoelastic constants.

Chapter 4

Strain Relaxation

4.1 Introduction

A variety of annealing experiments have been performed by other investigators in an attempt to better understand anisotropy in thin films. Smith et al [18] and Kneer and Zinn[19] have investigated the anisotropy in films of a non-magnetostrictive Ni-Fe composition. They annealed films in a magnetic field which was applied in the plane of the film perpendicular to the easy axis and observed the resulting changes in H_k with time for various annealing temperatures. By assuming that the observed changes in H_k were of the form:

$$H_k(t) + H_k(0) = H_1 e^{-t/t_1} + H_2 e^{-t/t_2} + \ldots \qquad (18)$$

where $t_i = t_{0i} e^{E_i/kT}$, the activation energies, E_i, for 3 to 6 independent processes involved were calculated. Unfortunately, these activation energies did not correspond to any known processes. Another approach by way of a simpler experiment was done by Finegan and Hoffman[10]. They measured the dependence upon annealing temperature of the isotropic strain which is found in thin films. However, no attempt was made to measure the activation energy of the process, so that no comparison with other known processes could be made.

In an attempt to understand the process of strain relaxation in thin films, uniaxially strained films were annealed at various temperatures for varying periods of time. These strained films were obtained

by evaporation onto bent substrates which resulted in uniaxially strained films on unstrained substrates. Upon annealing, the anisotropy of strained films changed by large amounts, but the anisotropy of unstrained films did not. It was found in Ch. 3 that the strain is proportional to the induced anisotropy. Thus the ratio of the induced anisotropy after annealing to that before annealing is inferred to be equal to the ratio of the strain after annealing to the initial strain. This ratio, the normalized strain, n, was measured as a function of annealing time t, annealing temperature T, and evaporation temperature T_e. From these results a single activation energy was calculated and correlated with results from bulk material.

4.2 Time and Temperature Dependence of Strain Relaxation

Significant changes in the normalized strain, n, were found for changes in annealing time and temperature. A typical plot of n as a function of annealing time with temperature as a parameter is shown in Fig. 7 for films evaporated at 25°C. Straight lines were drawn to best fit the data for each annealing temperature, which was taken by consecutive anneals of one film. It can be seen that the normalized strain is a very sensitive function of annealing temperature, while relatively insensitive to annealing time. Similar data were taken for films evaporated at seven temperatures between 100°C and 400°C. No dependence of n upon composition between 45% and 95% Ni-Fe and between 80% and 0% Ni-Co or upon initial strains between 5×10^{-4} and 10^{-3} was found.

The changes in n found with changes in t and T in Fig. 7 are very similar to the changes in H_k observed in perpendicular anneals by Smith et.al. Thus Eq. 18 can be used to describe n as a function of t and T

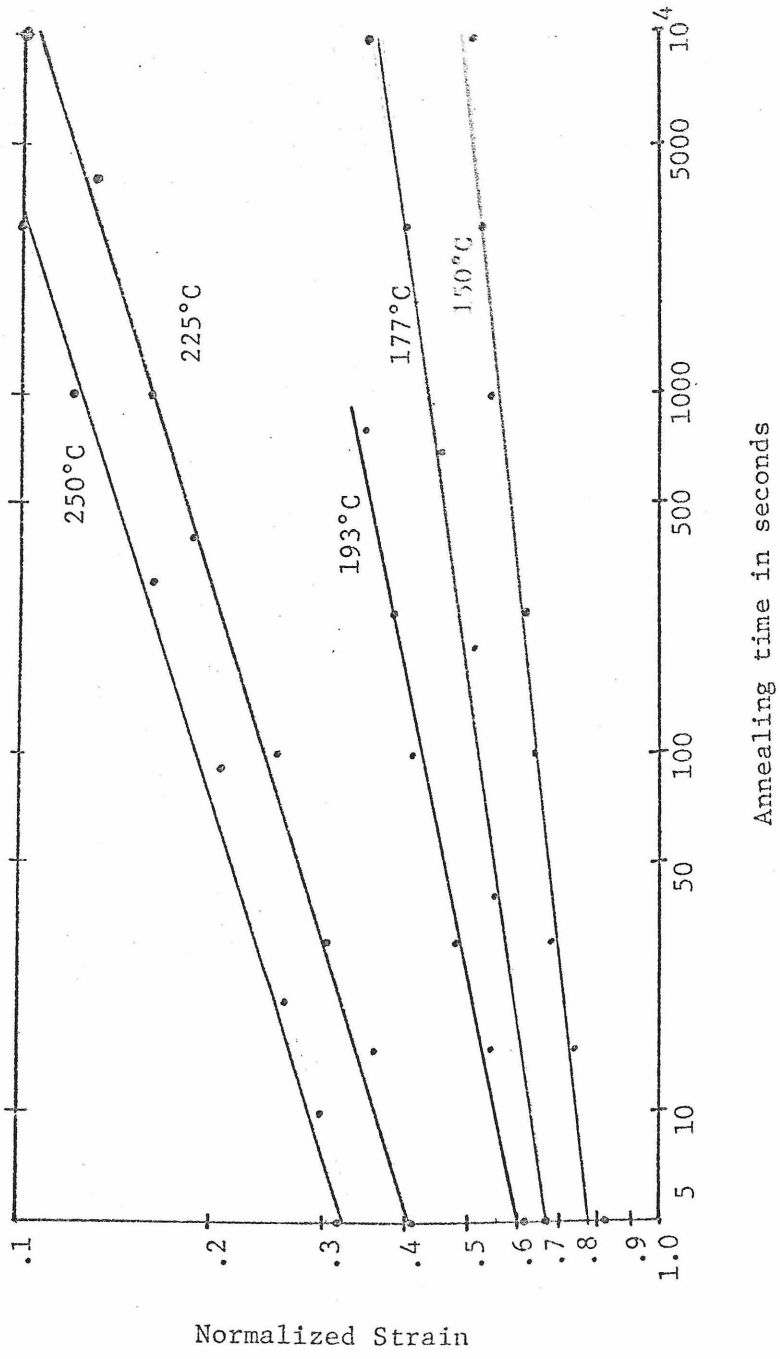

Fig. 7. The normalized strain as a function of annealing time for films evaporated at 25°C with annealing temperature as a parameter.

in terms of a sum of exponential processes. However, as found by Smith et.al., no unique set of activation energies can be found. Also, the data do not exhibit sharp changes in curvature as a function of t, as is characteristic for the thresholds of multiple independent processes. It is then reasonable to assume that a more complicated process rather than a sum of simple exponential processes exists. Even though the process is more complicated, it can be characterized by a single activation energy.

A single activation energy for strain relaxation, E_a, can be determined by plotting the data, not as in Fig. 7, but with n as a parameter. Figure 8 shows such a plot, where the time required to reach a constant value of n is plotted as a function of 1/T for films evaporated at 25°C, 100°C, 150°C, and 200°C. Here extrapolations of less than an order of magnitude were made to obtain points outside the experimental range. An exponential relation between annealing time and temperature results, which is characteristic of a single activation energy. Since each data point now represents data from a different film, the scatter is increased due to the differences between individual films. Due to this large scatter the functional dependence of the activation energy upon evaporation temperature could not be determined, even though E_a appears to increase with increasing evaporation temperature. This increase is most easily seen by comparing the slope of the data for T_e = 25°C (•) to the slope of the data for T_e = 200°C (x). From the line drawn to best fit all evaporation temperatures in Fig. 8, an activation energy of 2.4 ev $\pm$ .3 ev was calculated.

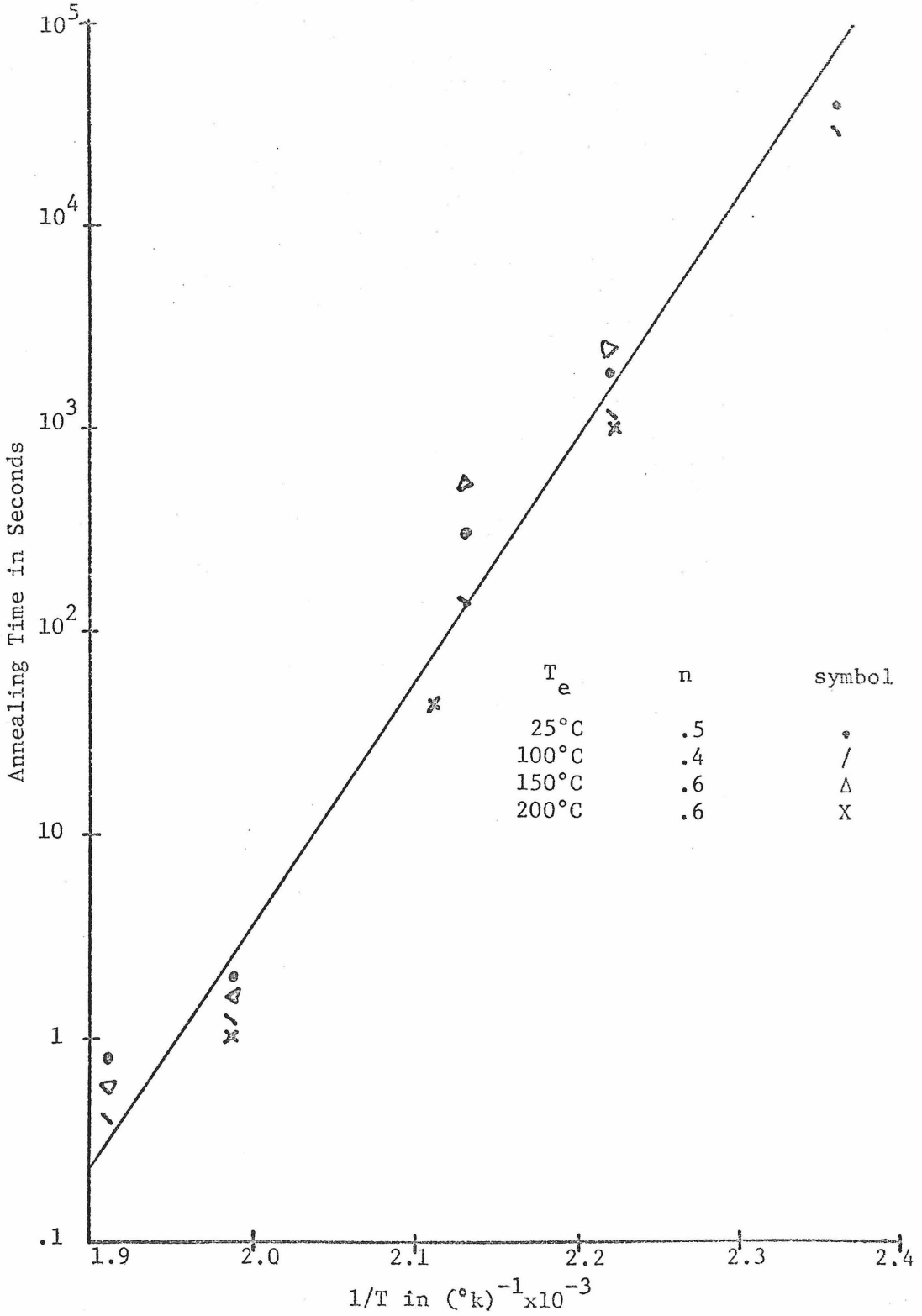

Fig. 8. Annealing time as a function of annealing temperature holding the normalized strain n constants for various evaporation temperatures T_e.

4.3 Dependence of n upon Evaporation Temperature

Significant differences in the strain relaxation rate were observed for different evaporation temperatures, T_e. To investigate the effect of T_e, consecutive three hour anneals at various annealing temperatures were done. These anneals give n as a function of annealing temperature with evaporation temperature as a parameter. Films evaporated at eight temperatures between 25°C and 400°C were annealed. Typical results are presented in Fig. 9 for films evaporated at 25°C and 200°C. Here each data point is the average for approximately 20 films. The lower the evaporation temperature, the more rapidly strain is relieved with increasing annealing temperature. However, the functional dependence of n upon T appears to be the same for all evaporation temperatures.

The activation energy characterizing the dependence of n upon T_e was found by an analysis similar to that used in Sec. 3.2. The rapid change of n with T near n = .5 allowed the annealing temperature at which n = .5, T(.5), to be determined accurately for all evaporation temperatures. Using these points, 1/T(.5) is plotted as a function of $1/T_e$ in Fig. 10. The error bars represent the uncertainty in the evaporation temperature (see Sec. 2.1). The resulting linear dependence of 1/T upon $1/T_e$ implies that n is some function of $E_a/T + E_e/T_e$ where $-E_e/E_a$ is the slope of the line drawn in Fig. 10 to best fit the data. Since E_a is an activation energy, it is reasonable to conclude that E_e is the activation energy related to the evaporation temperature. This activation energy can be calculated from the slope of Fig. 10 and E_a found in Sec. 3.2, giving E_e = 1 ev. Similar results obtained for

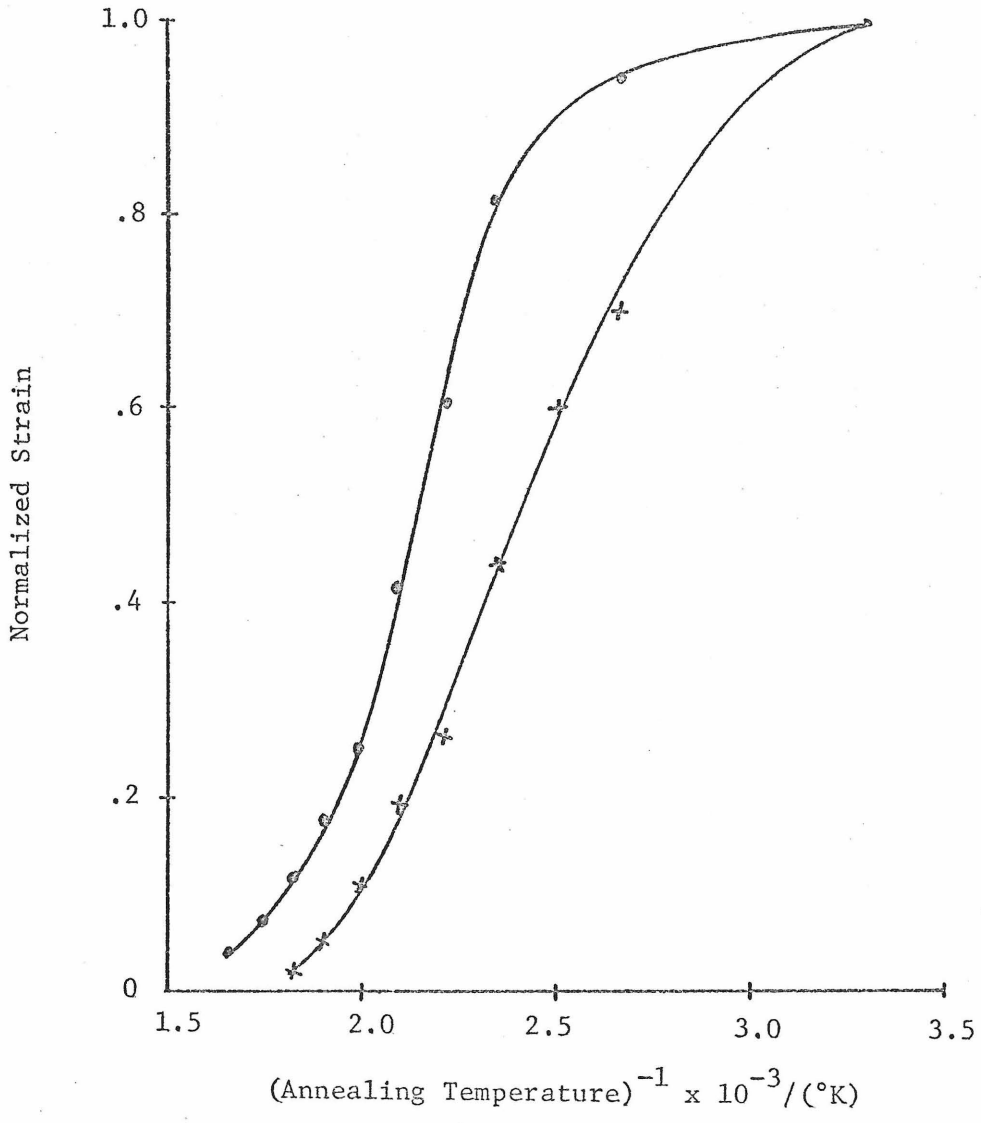

Fig. 9. Dependence of the normalized strain upon annealing temperature for consecutive 3 hr. anneals and evaporation temperatures of 25°C (X) and 200°C (•). Each data point represents approximately 20 films.

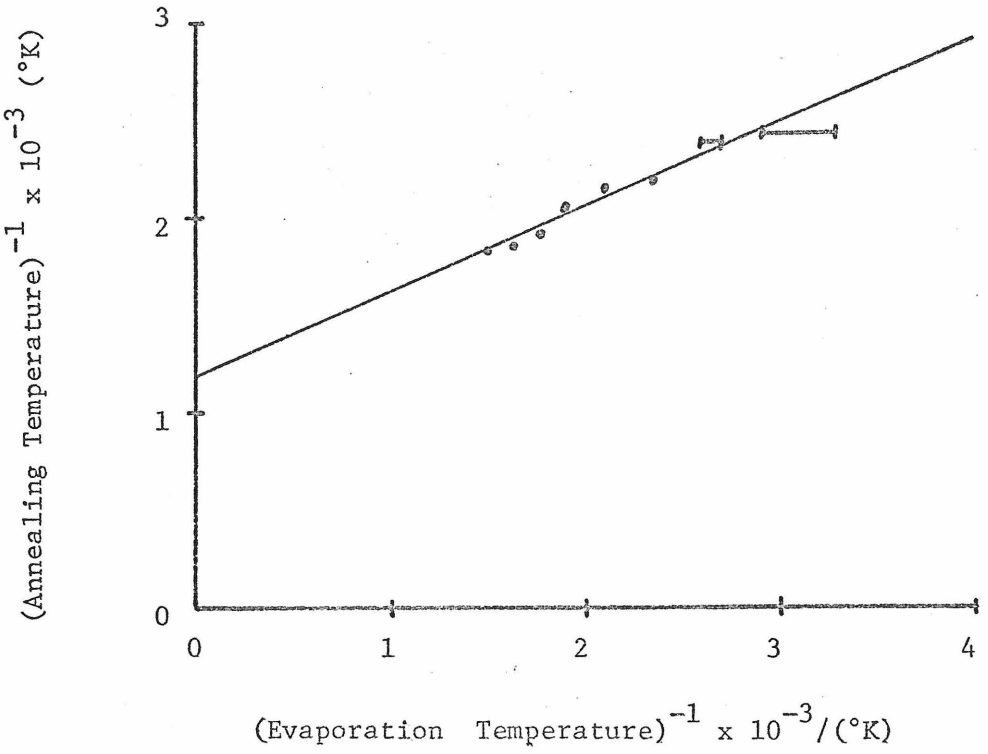

Fig. 10. The annealing temperature for which the normalized strain is .5 as a function of evaporation temperature.

other values of n confirm this value of E_e.

4.4 A Mechanism for Strain Relaxation in Thin Films

Different methods for calculating activation energies have been used for various annealing experiments. When the method used by Smith et al for finding activation energies was applied to the data from Secs. 4.2 and 4.3 for strain relaxation, a series of activation energies was found similar to that found by Smith et al for their perpendicular anneals. However, when the method described in Sec. 4.2 for finding activation energies is applied to Smith's data for perpendicular anneals a single activation energy can be found. Unfortunately, because of the design of his experiment where he changed annealing temperature and evaporation temperature together, the value of this single activation energy (0.5 ev) cannot be compared to an activation energy predicted for a single process. Unlike Smith's experiment, T was varied holding T_e constant when the process of strain relaxation was investigated. Thus the single activation energy found in Sec. 3.2 can be used to determine the mechanism dominating the process of strain relaxation.

A mathematical description of uniaxial strain relaxation by diffusional creep can be derived from the plastic strain rate for diffusional creep given by Chaudhari in Eq. 15. Since the isotropic strain, e_i, which exists in thin films is much larger than the applied uniaxial strain, e, it cannot be neglected in this case. The total strain in a film can be approximated by two large perpendicular strains, e_i and $e_i + e$. The change in the energy of formation of a vacancy due to these perpendicular strains is given by EVe_i and $EV(e_i+e)$ respectively, where

E is Young's modulus and V is the volume of a vacancy. By assuming $V=a^3$ where a is the lattice parameter, it can be shown that $EVe_i/kT>>1$ and that $EVe/kT<<1$ for typical values of e and e_i. These estimates simplify Eq. 18 so that it can be solved to give e_i and $e_i + e$ as functions of t and T. These equations can then be solved simultaneously for e. This solution in terms of n, where $n = e/e_o$ gives:

$$n = [1 + Hte^{(e_{io}VE-E_s)/kT}/kT]^{-1} \qquad (19)$$

where e_{io} is the initial isotropic strain and e_o is the initial uniaxial strain.

Equation 19 can be used to predict the results of strain relaxation annealing experiments. The activation energy, $E_a = E_s - EVe_{io}$, is expected to increase with increasing values of T_e, since e_{io} decreases with increasing evaporation temperature. By assuming $V = a^3$, the quantity EVe_{io} can be estimated to be less than 1 ev. and to change less than 0.5 ev. for normal changes in T_e. Then using the activation energy for volume diffusion (3 ev) for E_s, E_a should be between 2 and 3 ev and change less than 0.5 ev for normal values of T_e. This result was found experimentally. The average experimental activation energy found for normal evaporation temperatures is 2.4 ev , which is in good agreement with that predicted for volume diffusion dominating the process of strain relaxation.

Experimentally the dependence of n^3 upon t and T was found to be identical with the dependence predicted for n by Eq. 19. This type of functional difference for the predicted result from experiment could be caused by a non-linear stress-strain relation due to the large isotropic

strain, the appropriate elastic constants to use when calculating Eq. 19 are $E_i = S_i/e_i$ for the isotropic strain and $E = \Delta e_i$ for the uniaxial strain, where S_i is the isotropic stress.

From the results of Ch. 3, E can be estimated to be $E_i/2$. Using this estimate, n would become n^2 in Eq. 19, resulting in a more accurate prediction of n. Thus the difference between the predicted (Eq. 19) and experimental dependence of n upon t and T could be explained by the complexity of the process involved and does not reflect upon the mechanism of volume diffusional creep.

It has been shown that by using volume diffusional creep as a mechanism for strain relaxation in thin films, a simple model can be constructed (Eq. 19) to predict the experimental annealing behavior of uniaxial strain. This model assumes that films are only one crystallite in thickness and that the isotropic stress in thin films can be represented by two perpendicular stresses of equal magnitude. Both of these assumptions may be naive, making a more complex model necessary to accurately predict the experimental annealing behavior of strain relaxation. However, considering the accuracy with which the experimental activation energy and the functional dependence of n upon t and T was predicted by Eq. 19, it can be concluded that the process of strain relaxation in thin films is dominated by volume diffusional creep.

FOOTNOTES

1. A. G. Lesnik, G. I. Levin, and V. M. Nedostup, Phys. Stat. Sol. 17, 745 (1966).
2. E. N. Mitchell, G. I. Lykken, and G. D. Babcock, J. Appl. Phys. 715 (1963).
3. G. Robinson, J. of the Phys. Soc. Jap., 17, Sup. B-1, 558-567 (1962).
4. F. G. West, J. Appl. Phys. 35, 1827 (1964).
5. C. Kittel, Rev. Mod. Phys. 21, 541 (1949).
6. T. S. Crowther, J. Appl. Phys. 40, 1457 (1969).
7. P. Chaudhari, IBM J. Res. Develop., March 1969, 197.
8. C. Herring, J. Appl. Phys. 21, 437 (1950).
9. G. B. Gibbs, Phil. Mag. 13, 589 (1966).
10. J. D. Finegan and R. W. Hoffman, DTIE Microcard Issuance, January 19, 1962.
11. F. Humphrey, J. Appl. Phys. 38, 15-20 (1967).
12. L. W. Brownlow and C. H. Wilts, J. Appl. Phys. 41, 1250-1251 (1970).
13. R. M. Bozorth, Ferromagnetism, D. Van Nostrand, Co., 1961, 279, 109.
14. G. A. Alers, J. R. Neighbors, & H. Sato, J. Phys. Chem. Solids 13, 40 (1960).
15. F. Lichtenberger, Ann. Physik. 10, 45 (1932).
16. H. J. Leamy and H. Warlimont, Phys. Stat. Sol. 37, 523 (1970).
17. T. Suzuki and C. H. Wilts, J. Appl. Phys. 39, 6110 (1968).

18. D. O. Smith, G. P. Weiss, and K. J. Harte, J. Appl. Phys. 37, 1464 (1966).

19. G. Kneer and W. Zinn, Clausthal-Gottingen Proceedings of the International Symposium on Basic Problems in Thin Films Physics, p. 437 (1965).